Misch, D., Riedl, F., Liu, B., Horsfield, B., Ziegs, V., Mendez-Martin, F., Vranjes-Wessely, S., Sachsenhofer, R. F. (2019): Petrographic and sorption-based characterization of bituminous organic matter in the Mandal Formation, Central Graben (Norway). - *International Journal of Coal Geology*, *211*.

DOI: http://doi.org/10.1016/j.coal.2019.103229

Petrographic and sorption-based characterization of bituminous organic matter in the Mandal Formation, Central Graben (Norway)

Misch, D.[a*], Riedl, F.[a], Liu, B.[b], Horsfield, B.[c,d], Ziegs, V.[d], Mendez-Martin, F.[e], Vranjes-Wessely, S.[a], Sachsenhofer, R.F.[a]

[a)] Department of Applied Geosciences and Geophysics, Montanuniversitaet Leoben, A-8700

[b)] Northeast Petroleum University, Institute of Unconventional Oil and Gas, Daqing, China

[c)] GEOS4 GmbH, Michendorf, D-14552

[d)] GFZ German Research Centre for Geosciences, Potsdam, D-14473

[e)] Department of Materials Science, Montanuniversitaet Leoben, A-8700

**Corresponding Author:* David.Misch@unileoben.ac.at

Address: Department of Applied Geosciences and Geophysics - Chair of Petroleum Geology, Montanuniversitaet Leoben, Peter-Tunner-Straße 5, A-8700 Leoben

Key words: shale; organic petrography; solid bitumen; petroleum quality; sorption capacity; inner surface area; hydrocarbon retention

Research Highlights:

- Samples rich in vitrodetrinite are common both in marginal and basinal positions
- Coaly layers were exclusively found in the Søgne and Cod areas
- A correlation of TOC with liptinite percentages indicates enhanced bioproductivity or preservation efficiency
- Nitrogen sorption data indicate that the soluble organic matter fraction represents the controlling factor on micro- and mesopores
- Small mesopores are mainly associated with the high-molecular weight bituminous fraction, which appears non-porous at SEM-scale
- The total inner surface area decreases with thermal maturity

ABSTRACT

The Upper Jurassic Mandal Fm. of the Central Graben, Norway represents an important source rock that charged major petroleum accumulations in the North Sea, including the giant Ekofisk field. Nevertheless, exploration to date has been less successful than expected in marginal basin position such as the Cod Terrace, the Mandal High or the Søgne Basin, probably due to higher proportions of thermally stable (type III) kerogen. In an attempt to delineate changes in initial kerogen composition from later effects such as delayed expulsion of hydrocarbons, traditional organic petrography and scanning electron microscopy were combined with organic geochemical proxies and gas adsorption tests. The kerogen composition of the Mandal Fm. shows considerable variation. Samples hosting autochthonous coaly layers were found in wells from the Søgne Basin and the Cod Terrace, for which less generative potential was previously postulated. Nevertheless, samples hosting mainly vitrodetrinite were also found in basinal wells. A correlation of total organic carbon contents with liptinite percentages highlights enhanced bioproductivity or preservation efficiency for samples with abundant algal organic matter, that were likely deposited under deeper water and possibly oxygen-depleted conditions. By combining organic geochemical proxies with nitrogen sorption data, it could be proven that in case of the Mandal Fm., the (bituminous) organic matter fraction represents the controlling factor on abundance of micro- and mesopores and hence adsorptive gas retention. The amount of bitumen extractable from the Rock-Eval S2 peak ($S2_{bitumen}$) shows a strong correlation with the total inner surface area, suggesting that small mesopores (<10-15 nm) are mainly associated with the high-molecular bituminous fraction represented by the $S2_{bitumen}$, which appears non-porous at SEM-scale. Furthermore, the total inner surface area decreases strongly with thermal maturity, documenting a change in pore characteristics of the organic matter fraction (growth of mesopores and occurrence of macropores) by advancing hydrocarbon generation. Pyrobitumen-rich Upper Visean reference samples at peak oil and early wet gas window maturity show intense sponge-like pyrobitumen-hosted porosity coinciding with a low relative proportion of $S2_{bitumen}$ (high petroleum quality). Pyrobitumen is not affected by solvent extraction, thus not contributing high-molecular weight compounds to the extracted fraction. Such inert meso- to macroporous residues might contribute only relatively little to gas sorption capacity, but might represent important storage space for free gas, as well as flow pathways during expulsion.

1. Introduction

In many petroleum systems studies, the hydrocarbon source potential of organic matter-rich rocks is still mainly evaluated based on established bulk geochemical parameters (Peters et al., 1986). Apart from total organic carbon content (TOC), Rock-Eval pyrolysis is a standard technique for the fast determination of free hydrocarbon content (S1 peak), remaining hydrocarbon potential of the present kerogen (S2 peak), and thermal maturity (temperature of maximum hydrocarbon generation; T_{max}) at present state (Espitalie et al., 1977). Although more sophisticated methods like pyrolysis – gas chromatography (Py-GC) or fourier-transform ion cyclotron resonance mass spectrometry (FT-ICR-MS) vastly improved the understanding of organic matter transformation with ongoing burial and thermal maturation (Horsfield, 1989; Larter, 1984; Poetz et al., 2014; Ziegs et al., 2017), basic Rock-Eval parameters like the hydrogen index (HI) or the production index (PI) are still widely used to evaluate organic matter type and transformation stage. While this is reasonable considering that advanced characterization techniques are expensive, time consuming and not widely available, numerous studies showed that the aforementioned parameters have their limitations in terms of petroleum quality prediction (e.g., di Primio and Horsfield, 2006). Ziegs et al. (2017) showed for the Upper Jurassic Mandal Fm., that present (soluble) high-molecular weight hydrocarbons might contribute to the Rock-Eval S2 peak ($S2_{bitumen}$). This might lead to an overestimation of the remaining generative potential by Rock-Eval data. The S1 peak and corresponding PI, indicative for free hydrocarbons in the rock sample as well as the transformation ratio, is furthermore strongly affected by the expulsion efficiency (Cooles et al., 1986), controlled essentially by the retention behavior of present minerals and organic matter (primary macerals and secondary bitumen).

Ziegs et al. (2017) hence recommended the use of a new Rock-Eval parameter calculated as follows:

$$PQ = S1/TP$$

Whereby PQ denominates the petroleum quality, S1 the initial S1 peak from Rock-Eval measurements on whole rock samples (prior to solvent extraction) and TP the total petroleum content which is defined as the sum of the initial S1 peak and the $S2_{bitumen}$ determined by the equation:

$$S2_{bitumen} = S2_{whole\ rock} - S2_{extracted}$$

In an attempt to better understand the influence of primary organic matter type and secondary transformation products (as well as their selective retention) on these parameters, we combined traditional organic petrography with high-resolution scanning electron microscopy (SEM) and nitrogen gas adsorption tests. By comparing these data with the new Rock-Eval parameters determined for mostly early mature samples from the Mandal Fm., changes in sorptive storage capacity and visible organic matter-hosted porosity could be related to variations in primary maceral composition and the presence of $S2_{bitumen}$. The comparison with a set of peak oil mature Upper Visean reference samples, hosting similar (type III/II) kerogen and abundant nanoporous pyrobitumen, revealed maturity-related variations in petroleum quality.

The locally decreasing initial generative potential (e.g., Søgne Basin; see also Petersen et al., 2011) was assigned to variations in kerogen type. Hence, this work contributes to a refined organic matter typing and source potential assessment of the Mandal Fm., as well as a better understanding of the controls on petroleum expulsion efficiency from generative source rocks in general.

2. Geological Setting

Giant hydrocarbon accumulations in the North Sea are mainly sourced by Upper Jurassic marine shales (e.g., Huc et al., 1985; Baird, 1986; Cornford, 1998), comprising the Kimmeridge Clay and the Draupne, Spekk, Farsund and Mandal formations. Overlying the Haugesund and Farsund formations, the Mandal Fm. was deposited along the Norwegian and Danish Central Graben (Fig. 1), and gives name to the Mandal-Ekofisk(!) petroleum system (Cornford, 1994).

The regional setting in the late Permian – early Triassic was dominated by extension of the southern (Norwegian and Danish) parts of the Central Graben, which formed roughly NW-SE trending structural highs (e.g., Mandal & Hidra highs; Rossland et al., 2013) that separate the eastern Søgne Basin from the Feda Graben and the Breiflabb Basin (Petersen et al., 2011) (Fig. 1a). The Mandal Fm. was deposited in extensional depressions that were affected by syn-depositional salt tectonics related to the reactivation of Zechstein evaporites in the Upper Jurassic (Rossland et al., 2013).

The Upper Jurassic source rock succession in the Danish and Norwegian Central Graben has been investigated in great detail in terms of petroleum potential and resulting petroleum composition (e.g., di Primio and Horsfield, 2006). The depositional setting favored input of terrestrial plant material, especially in cases were turbidite currents transported continental debris from the graben flanks or structural highs to deeper positions in the basin center (Rossland et al., 2013). Nevertheless, a detailed organic petrographic characterization is missing for the Mandal Fm. in the study area. Charge of coarse clastics (and possibly higher land plant detritus) from the Mandal High continued until its flooding in Cretaceous times (Rossland et al., 2013), which also led to the formation of thick pelagic chalk deposits that act as major reservoirs for hydrocarbon accumulations (Ziegler, 1990).

The overlying Cenozoic syn- and post-rift succession shows a thickness of up to 4 km and includes mainly shallow-marine siliciclastic sediments with pelagic carbonates (Fig. 1b). This

sequence corresponds to subsidence caused by cooling due to the collapse of the North Sea Central Dome (Neumann, 2007) and increasing sediment load. Nevertheless, after the main extensional phase during the Middle and Upper Jurassic, rifting continued until the Paleocene (Holm, 1998), and cooling-induced subsidence is still active (Neumann, 2007).

The Mandal Fm. reaches the oil-generative stage at depths of 3600-4200 m in the central parts of the Central Graben (Cornford, 1994), hence the investigated sample set from a depth interval of 3400 – 4400 m is considered at early to peak oil window maturity. However, considerably diverging maturity trends were obtained from different areas in the Central Graben (e.g., the Søgne Basin; Petersen et al., 2011), where the Mandal Fm. apparently plays a minor role as hydrocarbon source.

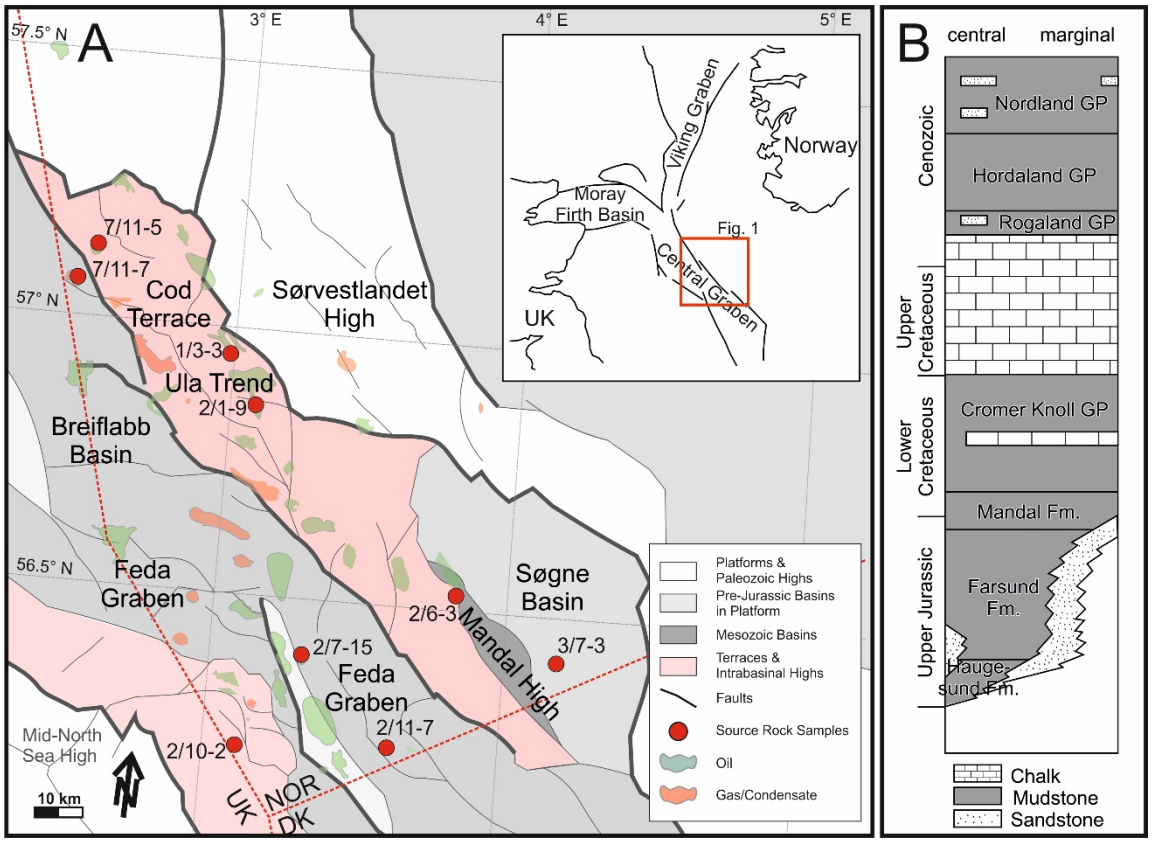

Fig. 1: (a) Regional setting of the study area and major structural features, locations of sampled wells, as well as major oil and gas fields. (b) Lithostratigraphic column for the central and marginal Central Graben (modified from Ziegs et al., 2017).

3. Samples and Methods

In total, 15 cuttings samples from 9 wells that drilled the Mandal Fm. in the Norwegian part of the Central Graben were investigated (well locations are shown in Fig. 1a). Due to the limited availability of cuttings samples suitable for organic petrographic and SEM investigations, no vertically well resolved succession could be studied. Nevertheless, samples were chosen from several key locations for which changing organofacies was previously postulated based on bulk geochemical data (e.g., Petersen et al., 2011), in order to cover those variations petrographically. Sampling depth, TOC, and Rock-Eval data of whole rock and solvent-extracted samples (after Ziegs et al., 2017) are given in Table 1. In addition, three peak oil mature samples from Upper Visean Rudov Beds (Ukrainian Dniepr-Donets Basin), hosting a similar type II/III kerogen and abundant nanoporous and likely remobilized (Misch et al., 2019) solid bitumen, were taken as a reference for the evaluation of petroleum quality ratings established by Ziegs et al. (2017), as well as for comparison of organic matter microstructures at SEM scale.

Table 1: Bulk geochemical and Rock-Eval parameters of Mandal Fm. samples before (whole rock) and after extraction (from Ziegs et al., 2017).

#	Well	Depth	Whole rock					Extracted						
			TOC wt.%	S1 mg/g	S2 mg/g	HI mg/g	Tmax °C	S1 mg/g	S2 mg/g	Tmax °C	S2bit mg/g	%bit %	TO mg/g	PQ
M-1	1/3-3	4070	6.8	4.48	13.41	197	433	0.04	5.92	439	7.49	56	11.97	0.37
M-2	2/10-2	3884	8.1	5.86	22.32	276	439	0.11	12.06	441	10.26	46	16.12	0.36
M-3	2/10-2	3887	8.23	6.46	22.7	276	436	0.07	11.66	440	11.04	49	17.5	0.37
M-4	2/10-2	3890	9.11	6.25	21.84	240	438	0.07	11.78	440	10.06	46	16.31	0.38
M-5	2/11-7	3775	10.4	8.78	46.71	449	432	0.1	30.82	430	15.89	34	24.67	0.36
M-6	2/11-7	3780	11.1	8.85	45.65	411	431	0.14	30.54	430	15.11	33	23.96	0.37
M-7	2/1-9	4023	4.44	3.79	11.41	257	449	0.05	5.69	448	5.72	50	9.51	0.40
M-8	2/1-9	4028	2.25	2.01	5.84	260	447	0.04	2.18	449	3.66	63	5.67	0.35
M-9	2/6-3	3412	5.01	1.72	23.49	469	429	0.02	16.53	432	6.96	30	8.68	0.20
M-10	2/6-3	3425	4.91	1.43	16.99	346	431	0.14	12.91	432	4.08	24	5.51	0.26
M-11	2/7-15	3587	2.69	1.12	6.73	250	435	0.03	3.98	437	2.75	41	3.87	0.29
M-12	3/7-3	3434	2.42	0.47	5.04	208	435	0.02	3.72	437	1.32	26	1.79	0.26
M-13	3/7-3	3500	2.83	0.53	5.31	188	435	0.02	3.96	436	1.35	25	1.88	0.28
M-14	7/11-5	4025	3.2	1.59	5.35	167	437	0.03	3.58	439	1.77	33	3.36	0.47
M-15	7/11-7	4420	8.28	2.89	9.16	111	440	0.04	5.02	445	4.14	45	7.03	0.41

TOC: total organic carbon; S1: free hydrocarbons; S2: hydrocarbons generated during Rock-Eval pyrolysis; HI: Hydrogen Index; Tmax: temperature of maximum hydrocarbon generation; S2bit – soluble fraction of S2 peak ($S2_{bitumen}$); %bit – S2 fraction related to $S2_{bitumen}$ (soluble) normalized to total S2; TO – total oil; PQ – petroleum quality

For organic petrographical investigations, samples were prepared as polished blocks following ASTM standards (ASTM, 2015). Primary and secondary organic matter (OM) types were identified by reflected light microscopy under oil immersion. Maceral percentages were determined semi-quantitatively by counting a total of 1000 measurement points per sample, using an automated point counter to avoid user bias. Microstructural investigations were conducted by high-resolution broad ion beam – scanning electron microscopy (BIB-SEM). For this, sub-samples were prepared by ion polishing with a Jeol IB-09010 BIB cross-section polisher that utilizes an argon ion beam (6 kV; 8 h), followed by a tungsten coating of ~7.5 nm to make the specimen conductive for high-resolution imaging. A FEI Versa 3D Dual Beam SEM was used for image acquisition.

Rock-Eval parameters were determined for the sub-set of three Rudov samples in untreated and solvent extracted condition (see also Ziegs et al., 2017). Representative portions of the whole rock samples were ground and subsequently extracted for 1 h using dichloromethane in a Dionex ASE 200 accelerated solvent extractor at 75°C and 75 bar. The extraction process was repeated two times to ensure that all soluble OM compounds were extracted. The amount of extractable OM (EOM) and the molecular composition of rock extracts (saturated, aromatic and heterocompound fractions) were then correlated with the SEM observations.

To evaluate the influence of organic matter composition on size distribution of mesopores and resulting inner surface area, gas adsorption tests were conducted on a sub-set of six samples using a Micromeritics ASAP 2460 surface area and porosity analyzer. Samples were crushed to 80 mesh and vacuum oven dried (105 °C; 10h) prior to analysis. Low pressure adsorption isotherms were then determined at 77 K, using nitrogen as adsorbate. Calculation of corresponding BJH (Barrett, Joyner and Halenda) average pore diameters, pore volumes

contributed by the pore fraction between 1.7 and 100 nm, and corresponding inner surface areas followed the approach of Barrett et al. (1951). Additionally, the pore volume contributed by pores in the range of 1.7 to 40 nm was calculated based on single-point BET (Brunauer, Emmett and Teller) estimations (Brunauer et al., 1940). It has to be emphasized that although widely used, both BET and BJH approaches are not recommended for use in heterogeneous, poorly defined microporous materials (Sing et al., 2001). As adsorption models relate to simplified pore geometries, the calculated equivalent pore size distributions are semi-quantitative at best. However, total pore volume and inner surface area might still be used for a relative comparison of pore characteristics within a set of similar samples.

4. Results

4.1 Organic petrography and bulk geochemical parameters

Semi-quantitative maceral and solid bitumen percentages from organic petrography are shown in Table 2. Maceral percentages vary considerably; vitrinite is the most abundant primary maceral group ranging between 7 and 89 vol% (avg. 38 vol%), followed by liptinite (0 – 70 vol%; avg. 23 vol%) and inertinite (0 – 35 vol%; avg. 10 vol%). Vitrodetrinite was found in all investigated wells in varying proportions, whereas coal particles comprising all three maceral groups in layers were exclusively observed in two samples from the Søgne Basin and the Cod Terrace (Fig. 2; see Fig. 1a for well locations).

Table 2: Maceral percentages for investigated Mandal Fm. samples.

#	Well	Depth	Macerals			
			Vitrinite vol.%	Liptinite vol.%	Inertinite vol.%	Solid bitumen vol.%
M-1	1/3-3	4070	41	14	9	36
M-2	2/10-2	3884	36	30	6	27
M-3	2/10-2	3887	39	6	2	53
M-4	2/10-2	3890	37	37	7	19
M-5	2/11-7	3775	9	55	5	32
M-6	2/11-7	3780	19	70	5	5
M-7	2/1-9	4023	14	0	5	81
M-8	2/1-9	4028	29	0	8	63
M-9	2/6-3	3412	21	59	21	0
M-10	2/6-3	3425	50	25	25	0
M-11	2/7-15	3587	89	11	0	0
M-12	3/7-3	3434	29	19	24	29
M-13	3/7-3	3500	88	7	0	5
M-14	7/11-5	4025	65	0	35	0
M-15	7/11-7	4420	7	7	0	87

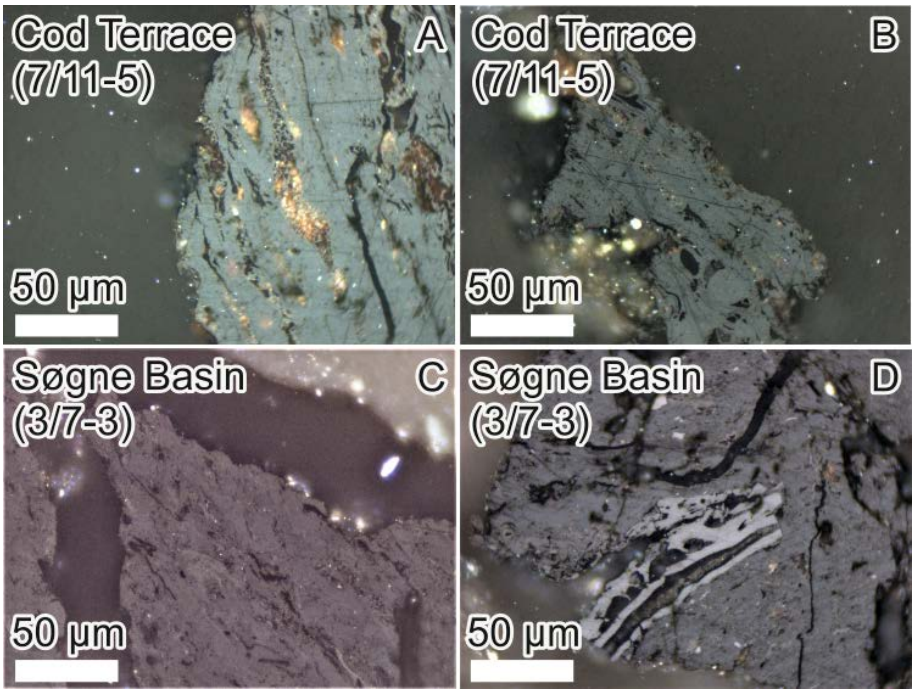

Fig. 2: (a, b) Coal particles in cuttings samples from well 7/11-5, located at the Cod Terrace. (c, d) Coal particles in cuttings samples from well 3/7-3 from the Søgne Basin.

Solid bitumen is abundant in most samples, ranging from 0 to 87 vol% (avg. 29 vol%). Excluding samples of elevated maturity (>445 °C Tmax), cumulative vitrinite and inertinite percentages show a negative correlation with TOC (R^2 ~ 0.57; Fig. 3a), whereas liptinite percentages show a weak positive trend (R^2 ~ 0.4; Fig. 3b). Solid bitumen percentages do not correlate with TOC values. Liptinite percentages follow a negative maturity trend against Tmax values (R^2 ~ 0.59; Fig. 3c). The decreasing visible liptinite percentages coincide with changing fluorescence color from yellow to orange-brown. The amount of solid bitumen shows a weaker positive trend with Tmax values (R^2 ~ 0.49; Fig. 3d), with the three peak mature samples >445 °C Tmax showing the highest petrographic solid bitumen percentages overall.

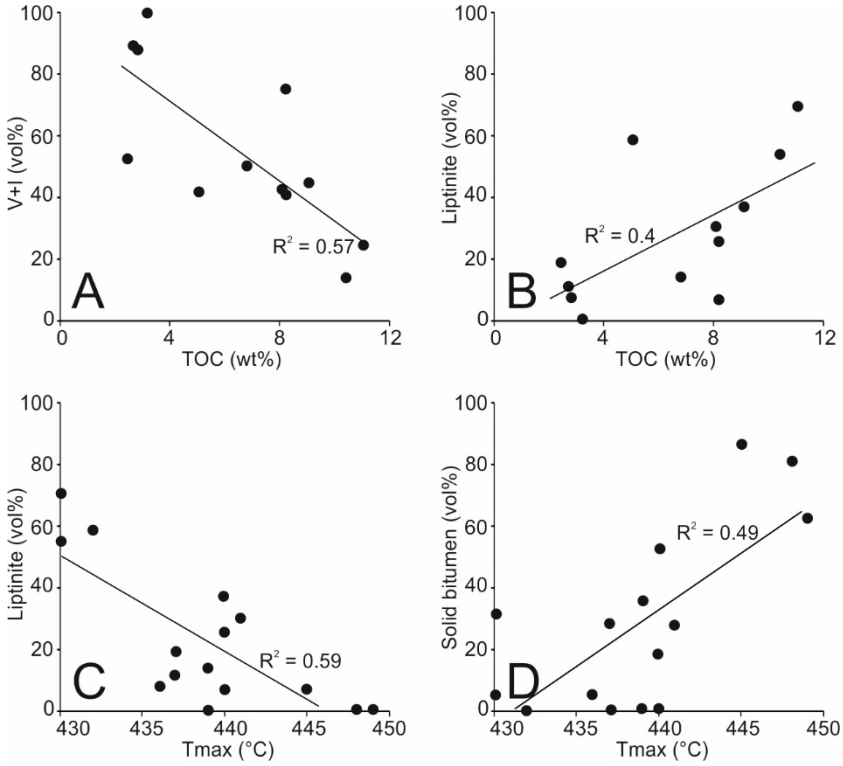

Fig. 3: (a) Correlation of total percentage of terrestrial macerals and TOC content. (b) Weak correlation of liptinite percentage and TOC content. (c) Correlation of liptinite percentage and Tmax from Rock-Eval pyrolysis. (d) Correlation of solid bitumen percentage and Tmax (note that petrographic solid bitumen and geochemical bitumen contents only show a weak correlation as seen in Fig. 4e). V – vitrinite; I – inertinite

The hydrogen index (HI) after solvent extraction correlates positively with liptinite percentages (R^2 ~ 0.78; Fig. 4a) and trends weakly negative with the total amount of terrestrial macerals (R^2 ~ 0.5; Fig. 4b). Similar trends were observed for the S1 determined on whole rock samples prior to solvent extraction. The amount of liptinite correlates positively with the S1 value (R^2 ~ 0.58; Fig. 4c), after exclusion of an outlier that shows the highest HI after solvent extraction. This sample also shows the overall lowest petroleum quality in absence of visible solid bitumen, pointing to a reduced S1 either due to retarded generation or anomalously early expulsion of free hydrocarbons. The total amount of terrestrial macerals shows a weak negative trend with S1 values (R^2 ~ 0.5; Fig. 4d). The percentage of petrographic solid bitumen shows almost no correlation with the percentage of $S2_{bitumen}$ normalized to the original S2 determined by Ziegs et al. (2017) (R^2 ~ 0.3; Fig. 4e), whereas no correlation with the total amount of petroleum (S1 + $S2_{bitumen}$) was observed (Fig. 4f). Vitrinite and liptinite do not show correlations with normalized $S2_{bitumen}$. The TOC content correlates with the unextracted S2 (R^2 ~ 0.71), the

238 $S2_{bitumen}$ and total oil (R^2 ~ 0.82 and 0.84, respectively), but not with normalized $S2_{bitumen}$ (Figs.

239 5a-d).

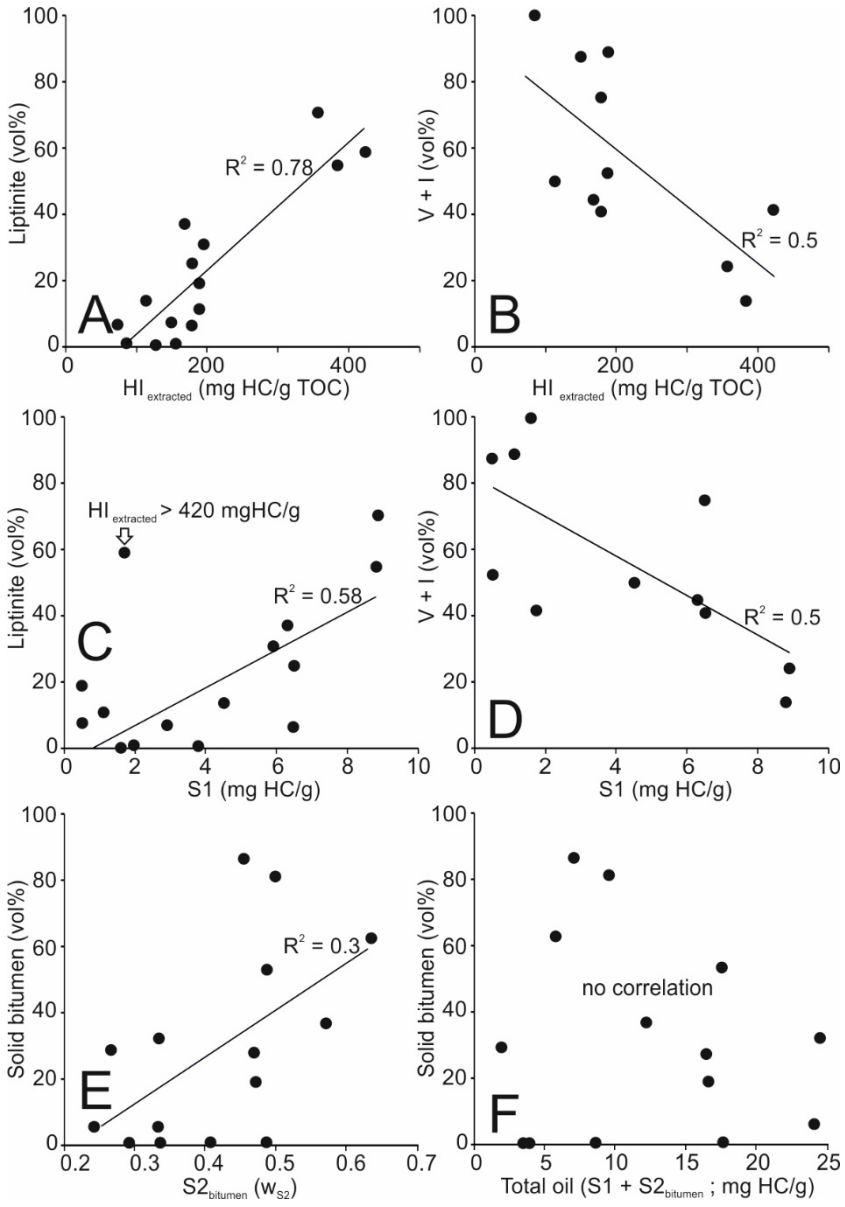

240

241 Fig. 4: (a, b) Trends of liptinite and cumulated amount of terrestrial macerals against the HI after solvent extraction.
242 (c, d) Weak trends of liptinite and cumulated amount of terrestrial macerals with the initial S1 peak. (e)
243 Almost no correlation between the amount of solid bitumen and the $S2_{bitumen}$ normalized to total S2. (f) No
244 correlation between petrographic solid bitumen percentage and total oil (S1 + $S2_{bitumen}$). V – vitrinite; I –
245 inertinite

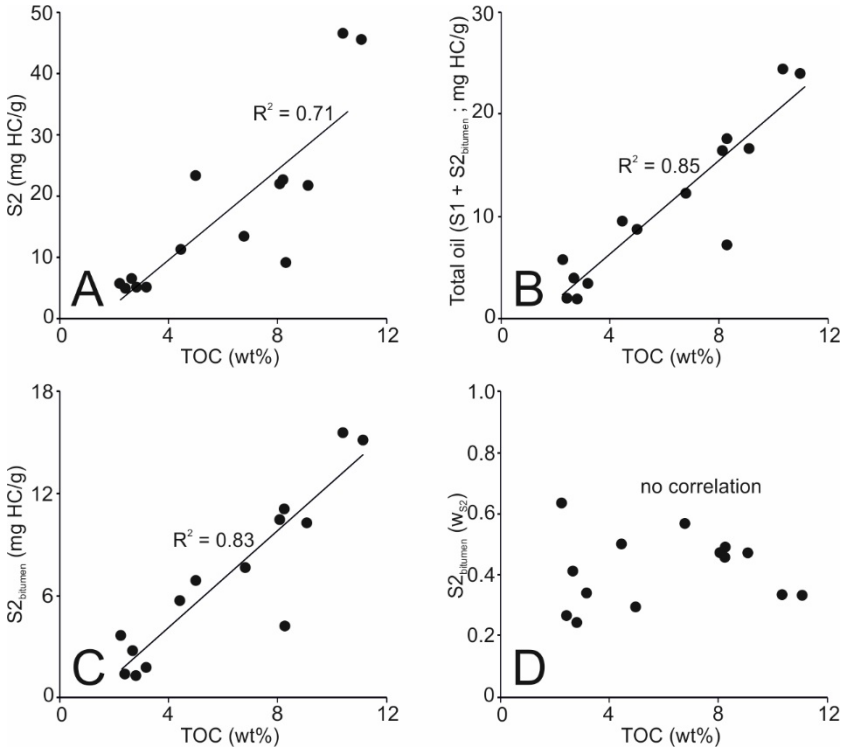

Fig. 5: (a) Correlation of TOC contents and S2 values. (b) Correlation of TOC contents and total oil (S1 + $S2_{bitumen}$). (c) Correlation of TOC contents and $S2_{bitumen}$. (d) No correlation between TOC contents and $S2_{bitumen}$ normalized to total S2.

4.2 Scanning electron microscopy

Following the nomenclature of Camp (2017), most of the organic matter visualized by SEM investigations appears amorphous and occurs both as laminae and disseminated void-filling organic matter (Fig. 6). Organic matter-hosted porosity in the SEM-visible range (>10-15 nm) is limited and mostly restricted to apparently void- or crack-filling organic matter that can be considered as secondary solid bitumen (Figs. 6e, f). Only few particles that according to their morphology might represent alginite macerals exhibit pores that are likely related to the primary organic matter structure (Fig. 6b). Most present organic matter pores are of secondary pendular or interface type (nomenclature after Loucks et al., 2012; Ko et al., 2017), whereas sponge-like porosity is relatively rare (Figs. 6h, i). There is no clearly visible maturity trend in organic matter-hosted porosity, and the petroleum quality (Ziegs et al., 2017) does in general not correlate with the frequency of pores either, although the sample with the highest petroleum quality (PQ = 0.5) shows some sponge-like pores in void-fillings and along laminae of

263 amorphous organic matter (Figs. 6g, h). Granular, intensely porous organic matter residues were

264 occasionally found in samples with low petroleum quality (<0.25) as well.

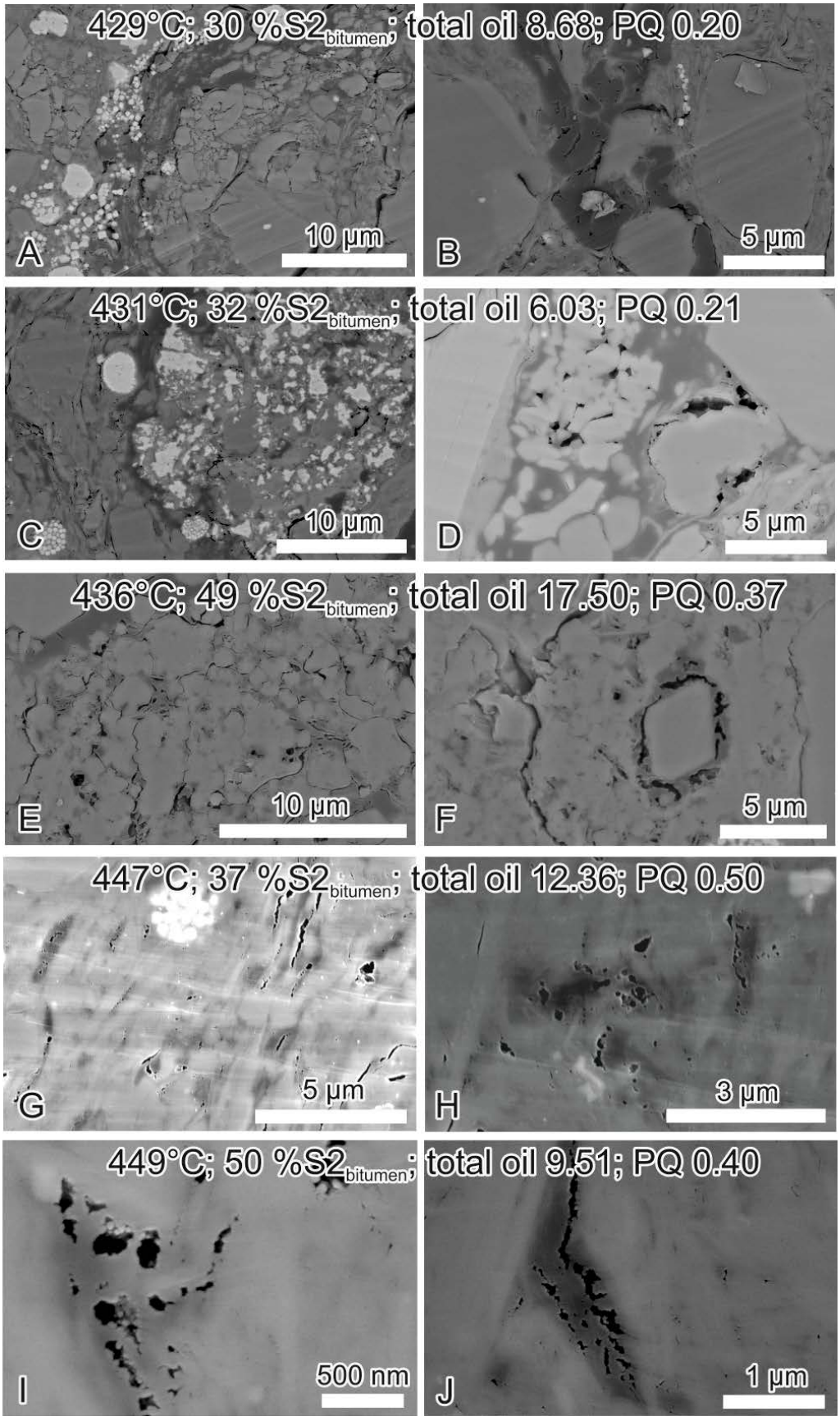

265

Fig. 6: (a-j) SEM (backscatter electron; BSE) images for selected samples of increasing maturity and varying petroleum quality. A clear maturity trend of SEM-visible organic matter porosity was not found for the investigated maturity range, although sponge-like solid bitumen pores seem to be more common in higher mature samples.

4.3 Nitrogen sorption isotherms

Nitrogen sorption isotherms for all investigated samples are shown in Fig. 7, whereas inner surface area and total pore volumes, as well as incremental pore volume distributions are highlighted in Figs. 8 and 9, respectively. Both immature and oil window mature samples of changing petroleum quality were chosen to cover possible maturity and organic matter-related trends.

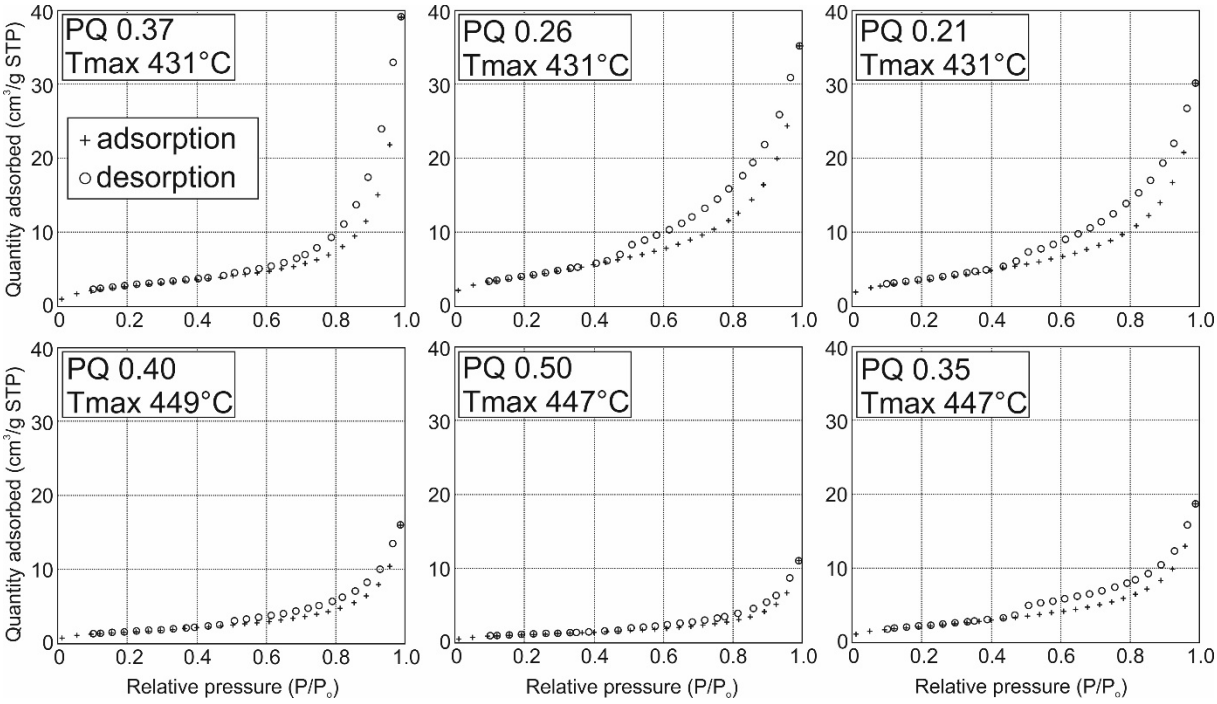

Fig. 7: Nitrogen adsorption and desorption isotherms of the investigated shales. The relative pressure refers to the ratio of vapor pressure of the analysis gas to the saturation vapor pressure. Note the comparably lower total adsorbed quantities at higher Tmax.

The average pore diameters calculated from the adsorption branch range between 13 and 23 nm, whereas the average pore diameters calculated from the desorption branch range between 10 and 18 nm, indicating dominant mesopores (2-50 nm). Both inner surface area and total pore volume of the pore class 1.7-100 nm calculated from the desorption branch by the BJH method proposed in Barrett et al. (1951) show wide variability from 4.9 to 21.6 m^2/g, and from 0.017 and 0.060 cm^3/g, respectively. The total pore volume calculated by BET single-point estimation

for the pore class 1.7 – 40 nm varies between 0.0095 and 0.036 cm^3/g. Inner surface area and total pore volumes correlate well with the measured Tmax value (R^2 ~ 0.7 and 0.88, respectively; Figs. 8a, c, d & 9), showing a decreasing trend with ongoing thermal maturation. Nevertheless, for samples at equal maturity, both parameters show considerable variability. A strong correlation (R^2 ~ 0.86) was furthermore found for the inner surface area and the petroleum quality (Fig. 8b).

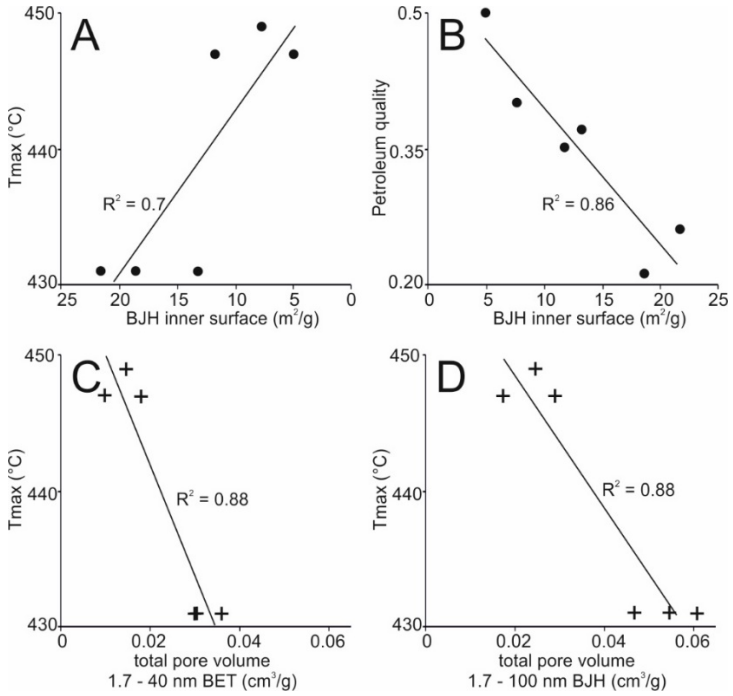

Fig. 8: (a) Correlation of cumulated BJH inner surface area calculated from the desorption branch of the nitrogen isotherm (Barrett et al., 1951) and Tmax. (b) Strong correlation of inner surface area and petroleum quality, suggesting that most micro- and mesoporosity occurs in high-molecular weight compounds represented by the $S2_{bitumen}$ fraction. (c) Correlation of the BET total pore volume (1.7 – 40 nm) and Tmax. (d) Correlation of the BJH total pore volume (1.7 – 100 nm) and Tmax.

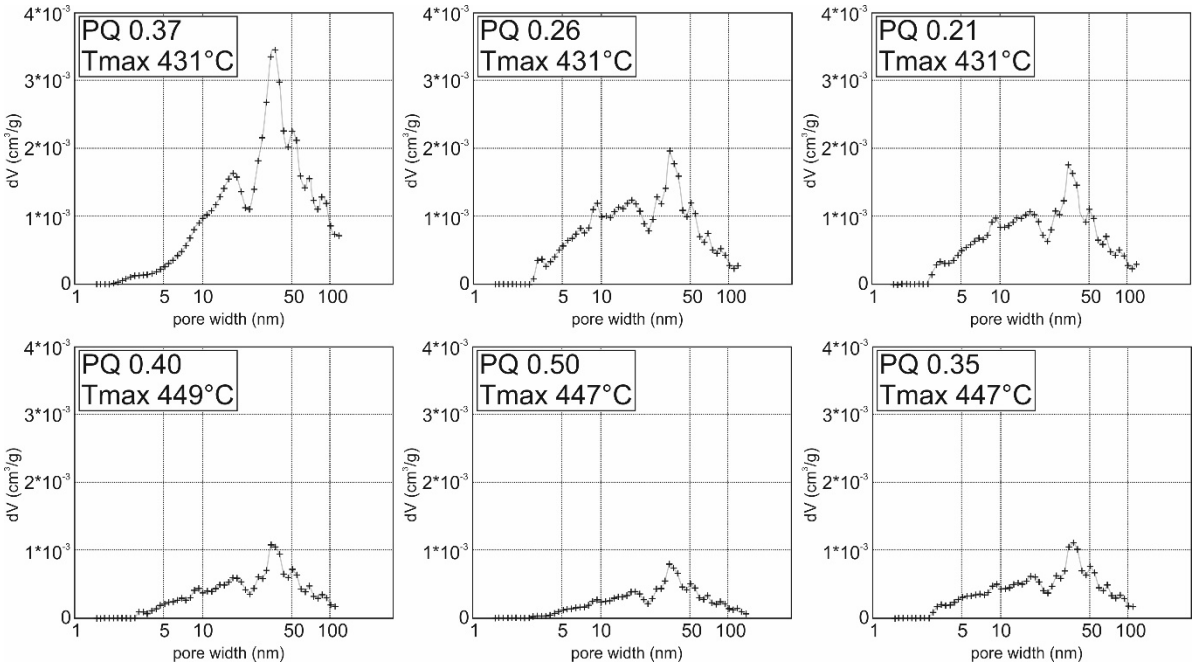

Fig. 9: Plots of incremental pore volume against pore diameter for the investigated shales. PQ – petroleum quality

4.4 $S2_{bitumen}$, petroleum quality and organic matter porosity of Upper Visean reference samples

TOC contents are given together with Rock-Eval parameters prior to and after solvent extraction in Table 3 for three Upper Visean reference samples. The initial Tmax values range between 458 and 463 °C, indicating higher thermal maturity compared to the investigated Mandal Fm. samples. This is confirmed by low HI values (83 – 96 mgHC/gTOC). The initial S1 values range between 1.2 and 2.1 mgHC/g, whereas the initial S2 values range between 3.2 and 5.4 mgHC/g. After solvent extraction, the S2 values are reduced to 2.7 – 4.8 mgHC/gTOC, resulting in $S2_{bitumen}$ percentages between 11 and 33 wt.% (see Table 3). The total petroleum ranges between 1.7 and 3.5 mgHC/gTOC, resulting in petroleum quality ratings of 0.6 to 0.71, which is considerably higher than for the less mature Mandal Fm. samples (Table 1).

Table 3: Bulk geochemical and Rock-Eval parameters of Upper Visean reference samples before (whole rock) and after extraction. $S2_{bitumen}$ (S2bit), total oil (TO) and petroleum quality (PQ) after Ziegs et al. (2017).

#	Whole rock					Extracted				Petroleum quality			
	TOC wt.%	S1 mg/g	S2 mg/g	HI mg/g	Tmax °C	S1 mg/g	S2 mg/g	Tmax °C	S2bit mg/g	%ker %	%bit %	TO mg/g	PQ
Pog74	3.75	1.19	3.20	85	463	0.25	2.73	464	0.47	85	15	1.65	0.72
Pog83	6.48	1.34	5.38	83	463	0.17	4.78	465	0.60	89	11	1.93	0.69

Yan195	4.34	2.08	4.21	97	458	0.06	2.83	463	1.38	67	33	3.45	0.60

TOC: total organic carbon; S1: free hydrocarbons; S2: hydrocarbons generated during Rock-Eval pyrolysis; HI: Hydrogen Index; Tmax: temperature of maximum hydrocarbon generation; S2bit – soluble fraction of S2 peak ($S2_{bitumen}$); %ker – S2 fraction related to kerogen (insoluble) normalized to total S2; %bit – S2 fraction related to $S2_{bitumen}$ (soluble) normalized to total S2; TO – total oil; PQ – petroleum quality

All three Upper Visean reference samples show abundant organic matter porosity (Fig. 10). Pendular (rim-forming) and interface pores, as well as sponge-like pores are present in all three samples. Partly, the samples show intense carbonate cementation and dissolution of quartz, indicated by pressure solution patterns in the microscale. Clay minerals that might represent primary matrix or secondary pore cements frequently intercalate with void-filling organic matter, thereby creating interface and pendular porosity (Figs. 10a, b). Most sponge-like pores are found in void-filling organic matter within interparticle pores preserved between detrital quartz grains (Figs. 10a, b). Furthermore, irregularly distributed clusters of sponge-like pores in larger laminae of amorphous organic matter that is interpreted as alginite (Fig. 10c) have been observed.

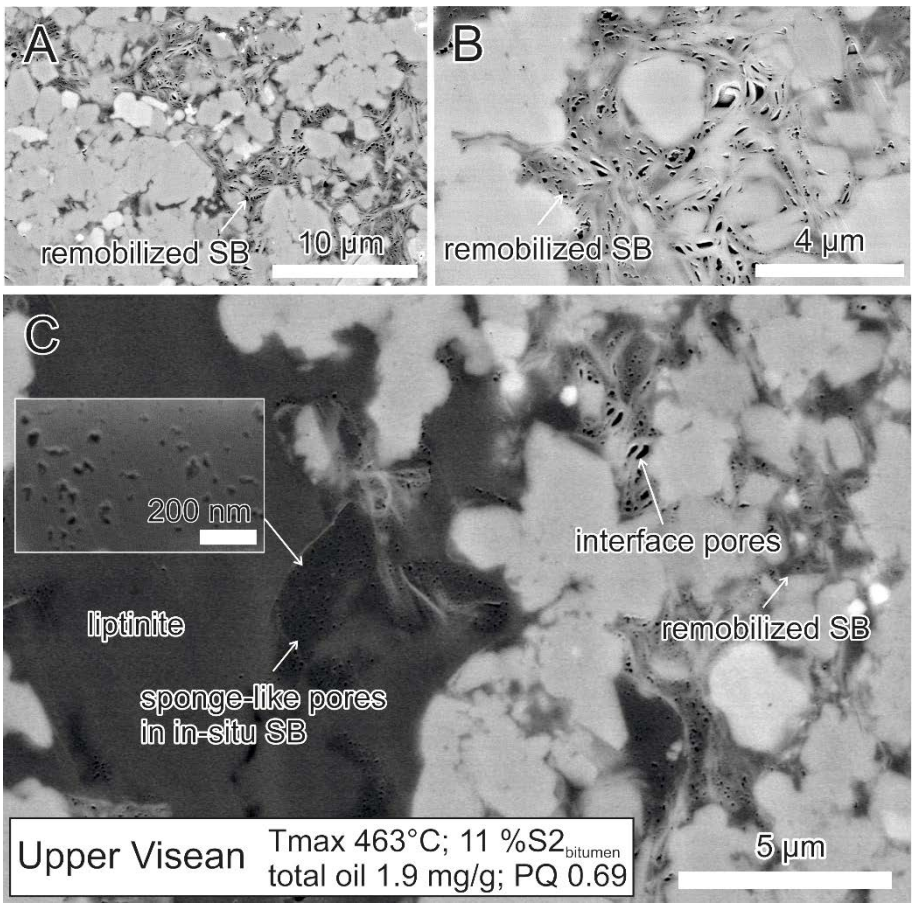

Fig. 10: (a, b) Remobilized solid bitumen residues filling interparticle pores in between quartz grains. Such porous residues often co-occur with clay minerals, forming additional pendular and interface pores. (c) Interpreted onset of solid bitumen formation within a primary liptinite particle. Nanopores indicate ongoing cracking of reactive kerogen into hydrocarbons. Note that the solid bitumen seems to be partly remobilized and accumulated in surrounding interparticle pores, intercalating with clay minerals. SB – solid bitumen; PQ – petroleum quality

5. Discussion

5.1 Influence of depositional setting on initial petroleum potential

The kerogen composition of the investigated samples from the Mandal Fm. shows considerable variation, implying changing generative potential. The HI after solvent extraction correlates with the percentage of liptinite (Fig. 4a), confirming the general reliability of semi-quantitative maceral analysis despite limitations inherent to the organic petrographical characterization of samples rich in finely dispersed solid bitumen. Terrestrially dominated samples rich in type III kerogen are not restricted to well locations near graben flanks or structural highs (Rossland et al., 2013); however, vitrinite in coaly layers that is interpreted as autochthonous was exclusively found in samples from the Søgne Basin and the Cod Terrace during this study (Fig. 2; for locations see Fig. 1a). For both locations, less generative potential and ~ 120 mgHC/gTOC decrease in original HI values compared to the more prolific wells in the Feda Graben was postulated (Petersen et al., 2011). This might be an indication that undercharging of traps and consequently less successful exploration in these areas might indeed be caused by higher contribution of more thermally stable type III kerogen as postulated by previous studies based on bulk geochemical data (e.g., Petersen et al., 2011; Rossland et al., 2013).

Considering the variability in kerogen proportions and the aforementioned good correlation of liptinite percentages with residual HI and S2 values after solvent extraction, the generative potential, but also hydrocarbon retention behaviour, have to be considered strongly influenced by changing initial kerogen composition. Furthermore, a correlation of TOC with liptinite percentages highlights enhanced bioproductivity or preservation efficiency for samples with abundant algal organic matter, that were likely deposited under deeper water and possibly more oxygen-depleted conditions during basin evolution.

5.2 Implications for hydrocarbon retention and expulsion efficiency

5.2.1 Hydrocarbon retention in mesopores

Previous studies showed that both mineralogy and organic matter composition strongly influence gas retention behaviour (Ross and Bustin, 2009; Mahlstedt and Horsfield, 2013; Han et al., 2015; Merkel et al., 2015). Clay minerals frequently host meso- and micropores within their internal structure, and hence mineralogy has to be considered an important factor to the understanding of retention behaviour in mature source rocks. Nevertheless, it is also accepted that in organic matter-rich successions, the type of organic matter present likely represents the main control on retention capacity (Cheng and Huang, 2004; Ziegs et al., 2017).

Ziegs et al. (2017) showed a positive gas retention trend with kerogen aromaticity and a negative correlation with HI values (Figs. 11a, b). Several authors postulate that as a consequence, the gas retention capacity of type III kerogen exceeds that of type II kerogen, as the proportion of high molecular weight aromatic compounds contributed to total petroleum (including soluble $S2_{bitumen}$) is higher in case of landplant-derived organic matter (Vandenbroucke and Largeau, 2007; Mo et al., 2008). In this study, we use the inner surface area as a measure of surface reactivity and hence sorption capacity of the present organic matter. While a decreasing trend of inner surface area against HI as described by Ziegs et al. (2017) for gas retention vs. HI (Figs. 11c, d) was not observed, a strong correlation ($R^2 \sim 0.86$) between the petroleum quality and the inner surface area from nitrogen sorption exists (Fig. 8b). At low petroleum quality ratings ≤ 0.2 (implying $> S2_{bitumen}$), the inner surface area is almost four times higher compared to samples showing a petroleum quality of 0.4 – 0.5 (see Fig. 8b). This difference is remarkable considering that organic matter only makes up for a small portion of whole rock samples. Hence, it seems reasonable that indeed in the investigated maturity range, sorptive gas storage is essentially controlled by the organic matter fraction. Assuming that type III kerogen tends to produce a higher proportion of high-molecular aromatic compounds during

petroleum generation (Mo et al., 2008), the trend of increasing inner surface area with decreasing petroleum quality (which corresponds to increasing bitumen aromaticity) supports the findings of Ziegs et al. (2017) based on gas retention determined by thermovaporization pyrolysis data. Data from this study suggests that sorptive gas retention is actually related to high-molecular weight bituminous organic matter ($S2_{bitumen}$), indicated by the strong correlation of inner surface area and petroleum quality. Small mesopores (2-10 nm) in such $S2_{bitumen}$ might contribute strongly to increasing inner surface area. Nevertheless, an additional contribution by micropores (<2 nm) in kerogen, which are not captured by nitrogen sorption, cannot be ruled out.

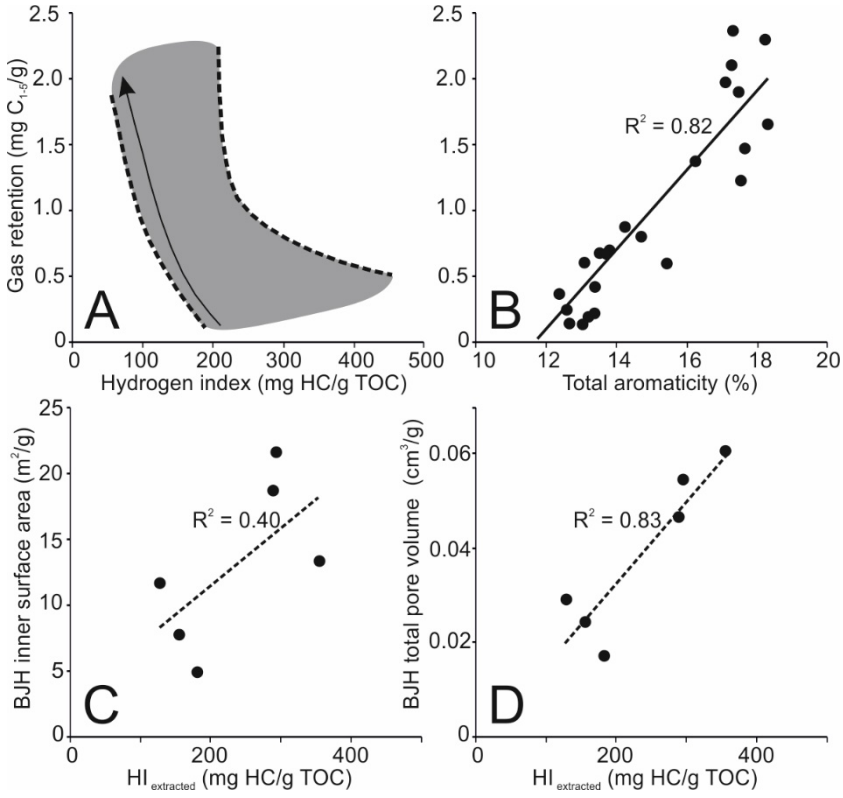

Fig. 11: (a, b) Negative gas retention trend with HI values (a) and positive trend with kerogen aromaticity (b) obtained by Ziegs et al. (2017) for the Mandal Fm. (c, d) In contrast, inner surface area (a) and total mesopore volume (b), suggested to control the gas sorption capacity, show a decreasing trend with HI values for the samples investigated during this study, pointing to a maturation overprint.

Apart from the abundance of high molecular weight $S2_{bitumen}$, a drastic change in the size of mesopores and hence inner surface area with thermal maturity was observed, with samples at 450°C Tmax showing only roughly half of the total inner surface compared to samples at 430°C Tmax. An increasing trend of sorption capacity against HI is visible (Figs. 11c, d), as opposed

401 to results in Ziegs et al. (2017), who assigned a negative trend of HI against gas retention to a
402 larger sample set from the Mandal Fm. (Fig. 11a). For the samples set investigated during this
403 study, the maturation-induced reduction of HI might impede its use as an indicator for kerogen
404 type. Hence, low HI values correlate with elevated maturity rather than abundant type III
405 kerogen that might provide aromatic sorption vacancies (Mo et al., 2008; Ziegs et al., 2017).
406 This is also supported by organic petrography (see Table 2). As gas production by primary and
407 secondary cracking progresses with ongoing thermal maturation, this effect of decreasing
408 sorptive retention capacity with advancing maturity needs to be taken into account when
409 evaluating the expulsion efficiency of sample sets covering a broad maturity interval.
410 Nevertheless, considerable scattering of retention capacity/inner surface area at equal maturity
411 supports a strong influence of the primary organic matter composition as described above.
412 Furthermore, selective preservation of clay mineral and organic matter pores as a function of
413 mineralogy and other influencing factors (e.g., pore pressure; Drews et al., 2018), as indicated
414 by changing mesopore characteristics in two samples that show considerably different
415 microstructure at equal thermal maturity (Fig. 12), might play a role.

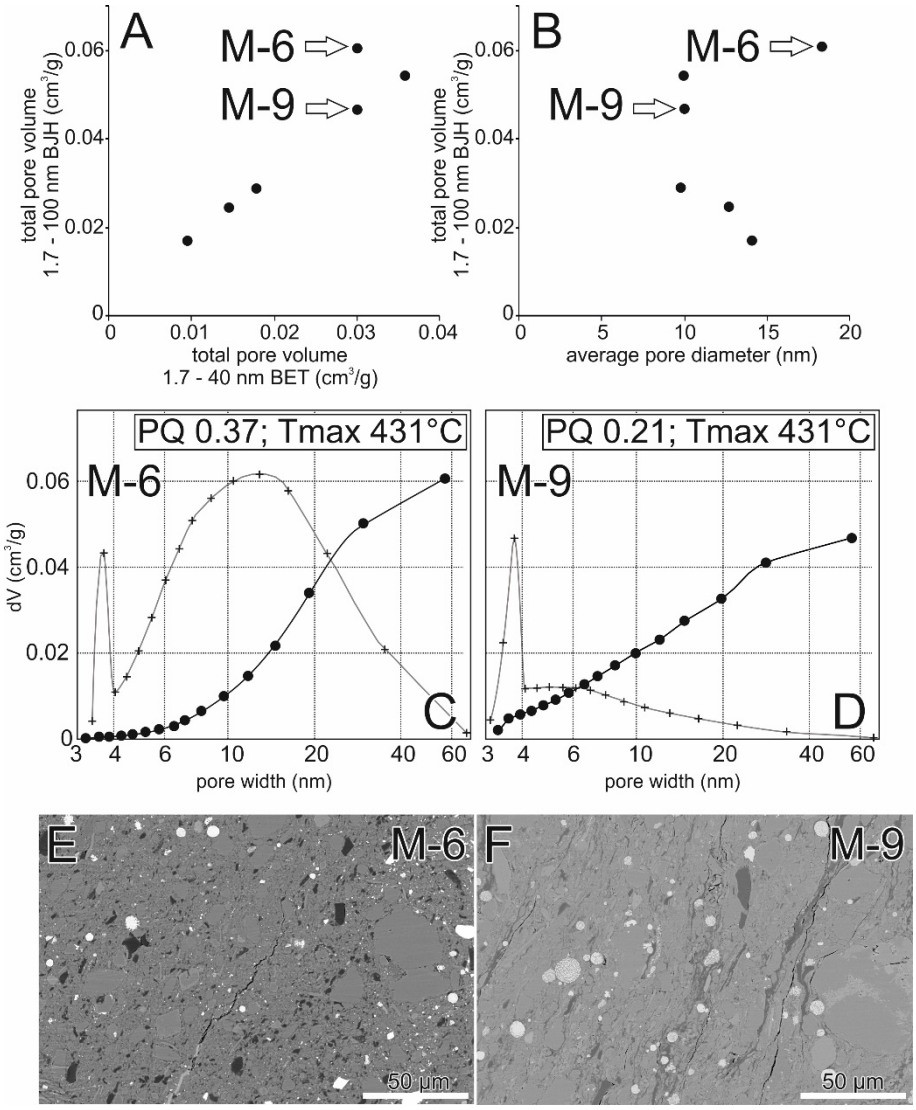

Fig. 12: (a) Dominance of pores in the range of 40 – 100 nm in a sample showing abundant brittle minerals and preserved nanopores in the clay mineral matrix (M-6). A sample with "normal" mesopore characteristics is highlighted for comparison (M-9). (b) Larger average mesopore diameter in sample (M-6) compared to sample (M-9). (c, d) BJH dV and cumulated pore volume distributions derived from the desorption branch of the nitrogen isotherm for both samples. (e, f) SEM images for both samples. Sample (M-6) shows abundant brittle minerals and comparably less lamination, as well as abundant preserved clay mineral nanoporosity. Matrix pores in sample (M-9) are mainly filled with organic matter, or not preserved due to more efficient compaction as indicated by more intense lamination.

5.2.2 Organic matter porosity evolution and controls on expulsion

Most SEM imaging studies actually postulate a higher abundance of sponge-like pores in (remobilized) pyrobitumen originating from an earlier mobile oil phase that migrated into open voids, or is formed in-situ along primary amorphous organic matter (e.g., Cardott et al., 2015; Mastalerz et al., 2018; Misch et al., 2019; Fig. 10). In general, liptinite-rich type II kerogens are considered more prone to the formation of such intensely porous solid bitumen residues (at SEM-scale) compared to relatively inert terrestrial type III kerogens (Misch et al., 2016;

Bernard et al., 2012; Cardott et al., 2015; Mastalerz et al., 2018). Type II kerogens should generate relatively more aliphatic petroleum, and hence the petroleum quality in such rocks should be higher. Furthermore, the petroleum quality should increase with ongoing cracking and consequent decrease in molecular weight of aromatic compounds. As a result of ongoing cracking, intensely nanoporous pyrobitumen residues, such as observed in the Upper Visean reference samples investigated here, are likely to form in open void space (e.g., Bernard et al., 2012). While this seems contradictory to the observed decreasing total pore volume and inner surface area with thermal maturity (Fig. 8a), it is important to note that the quantitatively detectable resolution of pores by modern image processing based on SEM techniques is in the range of ~ 30 nm ("practical resolution" acc. to Klaver et al., 2012; Misch et al., 2018). Most of the SEM-visible sponge-like pores in remobilized pyrobitumen originating from an earlier oil phase are actually in the large mesopore to macropore range, and consequently contribute comparably less to sorption capacity. A lower inner surface area at elevated thermal maturity in the Mandal Fm. samples is hence likely a result of larger mesopores in solid bitumen (Figs. 6h-j). Gas in such pores might be stored predominantly as free gas phase, and porous pyrobitumen networks might represent an important primary migration pathway within the source bed at advanced thermal maturity (Loucks et al., 2014; Cardott et al., 2015). Furthermore, the occlusion of both mineral matrix and organic matter pores might lead to an underestimation of organic porosity under the SEM (Loehr et al., 2015; Mastalerz et al., 2018; Xie et al., 2019). Loehr et al. (2015) postulated that both primary and secondary organic pores in oil window mature samples are mainly filled by liquid petroleum, hence not contributing to visible porosity. Xie et al. (2019) observed a similar effect for total effective porosity measured by petrophysical methods, which showed a substantial increase after solvent extraction. Misch et al. (2018) reported high saturated/aromatic compound ratios in source rock extracts of samples with abundant mesoporous pyrobitumen, and referred the dominance of saturated compounds to a lighter liquid hydrocarbon phase filling pores in inert pyrobitumen residues.

This study points to a complex pore structure of the bituminous organic matter fraction, which does not necessarily correlate with petrographically visible solid bitumen, as documented by the poor correlation shown in Fig. 4e. Abundant micro- and mesopores already at an immature stage (~430 °C Tmax) are documented by the strong control of present $S2_{bitumen}$ on the inner surface area. Nevertheless, primary organic matter meso- and macropores, which we observed mainly in liptinitic kerogen, as well as meso- and macropores in in-situ or remobilized solid bitumen derived from liptinitic kerogen, might play an important role in the retention of liquid hydrocarbons (Loehr et al., 2015), although they might not contribute to the total effective porosity if occluded by hydrocarbons (Xie et al., 2019).

5.3 Comparison between organic geochemical and petrographical organic matter typing

The presented data reflects some ambiguities that arise from the varying definitions of bitumen in organic geochemistry and petrography (Katz and Arango, 2018; Mastalerz et al., 2018; Misch et al., 2019), as well as the limitations in delineation of primary kerogen and (in-situ) bitumen by organic petrography. We found it impossible to petrographically distinguish samples rich in $S2_{bitumen}$ (bitumen retained in kerogen) petrographically both by optical microscopy and SEM. Petrographic solid bitumen shows almost no trend with normalized $S2_{bitumen}$ (R^2 ~ 0.3; Fig. 4e) or total oil from organic geochemistry, whereas liptinite or vitrinite percentages do not show a correlation with those parameters at all (Fig. 4). The sample with the highest HI after solvent extraction and lowest petroleum quality (0.2) at ~ 30% of bitumen fraction in the S2 peak shows no petrographically identifiable solid bitumen and no clearly void-filling solid bitumen under the SEM, indicating that this fraction of geochemical bitumen is actually retained directly in the kerogen or at least forms an entity that cannot be petrographically resolved. While at a higher maturity stage void-filling remobilized and often porous solid bitumen might be visually identifiable (Fig. 10), only an indirect correlation of petroleum quality (and hence amount of

$S2_{bitumen}$) and the inner surface area from adsorption measurements supports the geochemical data in case of early mature samples with abundant $S2_{bitumen}$. On the other hand, porous solid bitumen in the Upper Visean reference samples that was clearly identified by both optical microscopy and SEM did not cause a poor petroleum quality (petroleum phase rich in high-molecular $S2_{bitumen}$), probably due to its low solubility in organic solvents. As it is impossible to differentiate between soluble and insoluble solid bitumen petrographically, and geochemical parameters only respond to the soluble bitumen fraction (and are hence not sensitive to abundant pyrobitumen), we propose to combine both petrographical and geochemical data for improved organic matter typing in the presence of considerable amounts of primary or secondary amorphous organic matter (Cardott et al., 2015; Camp, 2017). Structural characterization by combined high-resolution imaging and gas adsorption tests turned out as a valuable tool towards a better understanding of retention and expulsion characteristics. Nevertheless, the combination with traditional organic petrography was found crucial to distinguish between influences from variations in primary kerogen composition and later compositional changes caused by thermal maturation.

6. Conclusions

This work follows up on the extensive geochemical study conducted by Ziegs et al. (2017) on the Mandal Fm. of the Central Graben, Norway. It provides new petrographic evidence for the deposition of coaly layers along structural high zones in the Upper Jurassic, and contributes to a better understanding of storage and expulsion behaviour as a function of organofacies and ongoing thermal maturation.

The key findings of this study area summarized below:

- The kerogen composition of the Mandal Fm. shows considerable variation. Type III-rich samples hosting high proportions of vitrodetrinite are not restricted to positions near graben flanks or structural highs, but also occur in basinal wells, thereby influencing generative potential and gas retention behaviour.
- Layers of autochthonous vitrinite were exclusively found in the Søgne and Cod areas, for which a lower generative potential was previously postulated based on organic geochemical evidence.
- A decreasing trend of TOC with total amount of terrestrial macerals and a corresponding weak increasing trend with liptinite content might indicate enhanced bioproductivity or preservation efficiency for samples with abundant algal organic matter, that were likely deposited under deeper water conditions.
- Nitrogen sorption data indicates that the organic matter fraction represents the main controlling factor on micro- and mesopores and hence adsorptive gas retention.
- Petroleum quality and corresponding amount of $S2_{bitumen}$ show a strong correlation with the total inner surface area, suggesting that small mesopores (2-10 nm) are mainly associated with the high-molecular weight bituminous fraction, which appears non-porous at SEM-scale.

- The total inner surface area decreases with thermal maturity, pointing to a change in pore characteristics (growth of mesopores and occurrence of macropores due to ongoing cracking).
- Pyrobitumen-rich Upper Visean reference samples at peak oil and early wet gas window maturity show intensely porous solid bitumen coinciding with a high petroleum quality, suggesting that these porous residues are actually not affected by solvent extraction. Such meso- to macroporous residues (that are clearly visible in SEM) might contribute only relatively little to gas sorption capacity, but might represent important storage space for free gas, as well as flow pathways during expulsion.

Acknowledgments

Gerhard Hawranek (Chair of Physical Metallurgy, Montanuniversitaet Leoben) is thanked for help with the acquisition of SEM images. Thoughtful comments of the journal editor and two anonymous reviewers are gratefully acknowledged. This work was funded by the Austrian science fund FWF (grant no. P 29310-NBL).

References

ASTM International, 2015. ASTM D2797/D2797M-11a: Standard practice for preparing coal samples for microscopical analysis by reflected light. ASTM International, West Conshohocken, Pennsylvania, 5 p.

Baird, R.A., 1986. Maturation and source Rock-Evaluation of Kimmeridge clay, Norwegian North Sea. AAPG Bulletin, 70, 1-11.

Barrett, E.P., Joyner, L.G., Halenda, P.P., 1951. The Determination of Pore Volume and Area Distributions in Porous Substances. I. Computations from Nitrogen Isotherms. Journal of the American Chemical Society, 73, 373-380.

Bernard, S., Wirth, R., Schreiber, A., Schulz, H.M., Horsfield, B., 2012. Formation of nanoporous pyrobitumen residues during maturation of the Barnett Shale (Forth Worth Basin). International Journal of Coal Geology, 103, 3-11.

Brunauer, S., Deming, L.S., Deming, W.S., Teller, E., 1940. On a theory of the van der Waals adsorption of gases. Journal of the American Chemical Society, 62, 1723-1732.

Cardott, B.J., Landis, C.R., Curtis, M.E., 2015. Post-oil solid bitumen network in the Woodford Shale, USA – A potential primary migration pathway. International Journal of Coal Geology, 139, 106-113.

Camp, W.K., 2017. Strategies for identifying organic matter types in SEM. SEPM-AAPG Hedberg Research Conference, Mudstone Diagenesis, Santa Fe, New Mexico, Oct. 16-19, 2016. AAPG Datapages Search and Discovery Article #70233.

Cheng, A.-L., Huang, W.-L., 2004. Selective adsorption of hydrocarbon gases on clays and organic matter. Organic Geochemistry, 35, 413-423.

Cooles, G.P., Mackenzie, A.S., Quigley, T.M., 1986. Calculation of petroleum masses generated and expelled from source rocks. Organic Geochemistry, 10, 235-245.

Cornford, C., 1994. Mandal-Ekofisk(!) petroleum system in the Central Graben of the North Sea. In: Magoon, L.B., Dow, W.G. (Eds.), The petroleum system - From source to trap. AAPG Tulsa, Oklahoma, 537-571.

Cornford, C., 1998. Source rocks and hydrocarbons of the north sea. In: Glennie, K.W. (Ed.), Petroleum Geology of the North Sea: Basic Concepts and Recent Advances, Blackwell Sci. Ltd. (fourth ed.), Oxford (United Kingdom), 376-462.

Drews, M., Bauer, W., Caracciolo, L., Stollhofen, H., 2018. Disequilibrium compaction overpressure in shales of the Bavarian Foreland Molasse Basin: Results and geographical distribution from velocity-based analyses. Marine and Petroleum Geology, 92, 37-50.

di Primio, R., Horsfield, B., 2006. From petroleum-type organofacies to hydrocarbon phase prediction. AAPG Bulletin, 90, 1031-1058.

Espitalié, J., Laporte, J., Madec, M., Marquis, F., Leplat, P., Paulet, J., Boutefeu, A., 1977. Méthode rapide de caractérisation des roches mètres, de leur potentiel pétrolier et de leur degré d'évolution. Oil & Gas Science and Technology, 32, 23-42.

Han, Y., Mahlstedt, N., Horsfield, B., 2015. The Barnett Shale: Compositional fractionation associated with intraformational petroleum migration, retention and expulsion. AAPG Bulletin, 99, 2173-2202.

578 Holm, G. M., 1998. Distribution and origin of overpressure in the Central Graben of the North
579 Sea: Abnormal pressures in hydrocarbon environments, In: Law, B.E., Ulmishek, G.F.,
580 Slavin, V.I. (Eds.), Distribution and Origin of Overpressure in the Central Graben of
581 the North Sea, AAPG Memoir, 70, 123-144.

582 Horsfield, B., 1989. Practical criteria for classifying kerogens: Some observations from
583 pyrolysisgas chromatography. Geochimica et Cosmochimica Acta, 53, 891-901.

584 Huc, A.-Y., Irwin, H., Schoell, M., 1985. Organic matter quality changes in an Upper Jurassic
585 shale sequence from the Viking Graben, In: Thomas, B.M., Doré, A.G., Eggen, S.,
586 Home, P.C., Larsen, R.M. (Eds.), Petroleum geochemistry in exploration of the
587 Norwegian Shelf. Graham & Trotman, for Norwegian Petroleum Society, London, 179-
588 183.

589 Katz, B.J., Arango, I., 2018. Organic porosity: a geochemist's view of the current state of
590 understanding. Organic Geochemistry, 123, 1-16.

591 Klaver, J., Desbois, G., Urai, J.L., Littke, R., 2012. BIB-SEM study of the pore space
592 morphology in early mature Posidonia Shale from the Hils area, Germany. International
593 Journal of Coal Geology, 103, 12-25.

594 Ko, L.T., Loucks, R.G., Ruppel, S.C., Zhang, T., Peng, S., 2017. Origin and characterization of
595 Eagle Ford pore networks in the south Texas Upper Cretaceous shelf. AAPG Bulletin,
596 101, 387-418.

597 Larter, S.R., 1984. Application of analytical pyrolysis techniques to kerogen characterization
598 and fossil fuel exploration/exploitation. In: Voorhees, K. (Ed.), Analytical Pyrolysis -
599 Methods and Applications. Based upon the invited lectures presented at the Fifth
600 International Symposium on Analytical Pyrolysis. Butterworths, London, 212-275.

601 Loehr, S.C., Baruch, E.T., Hall, P.A., Kennedy, M.J., 2015. Is organic pore development in gas
602 shales influenced by the primary porosity and structure of thermally immature organic
603 matter?. Organic Geochemistry, 87, 119-132.

604 Loucks, R.G., Reed, R.M., Ruppel, S.C., Hammes, U., 2012. Spectrum of pore types and
605 networks in mudrocks and a descriptive classification for matrix-related mudrock pores.
606 AAPG Bulletin, 96, 1071-1098.

607 Loucks, R.G., Reed, R.M., 2014. Scanning-electron-microscope petrographic evidence for
608 distinguishing organic-matter pores associated with depositional organic matter versus
609 migrated organic matter in mudrocks. GCAGS Journal, 3, 51-60.

610 Mahlstedt, N., Horsfield, B., 2013. A new screening tool for the rapid evaluation of gas sorption
611 capacity in shales. In: Jin, Z., Katz, B.J. (Eds.), AAPG Hedberg. AAPG Beijing, China.

612 Mastalerz, M., Drobniak, A., Stankiewicz, A.B., 2018. Origin, properties, and implications of
613 solid bitumen in source-rock reservoirs: A review. International Journal of Coal
614 Geology, 195, 14-36.

615 Merkel, A., Fink, R., Littke, R., 2015. The role of pre-adsorbed water on methane sorption
616 capacity of Bossier and Haynesville shales. International Journal of Coal Geology, 147-
617 148, 1-8.

618 Misch, D., Mendez-Martin, F., Hawranek, G., Onuk, P., Gross, D., Sachsenhofer, R.F., 2015.
619 SEM and FIB-SEM investigations on potential gas shales in the Dniepr-Donets Basin
620 (Ukraine): pore space evolution in organic matter during thermal maturation. IOP
621 Conference Series: Materials Science and Engineering, 109, paper 012010.
622 https://doi.org/10.1088/1757-899X/109/1/012010

Misch, D., Klaver, J., Gross, D., Rustamov, J., Sachsenhofer, R.F., Schmatz, J., Urai, J.L., 2018b. Pore space characteristics of Upper Visean "Rudov Beds": Insights from BIB-SEM and organic geochemical investigations. Geological Society, London, Special Publications, 484, 24pp.

Misch, D., Gross, D., Hawranek, G., Horsfield, B., Klaver, J., Mendez-Martin, F., Urai, J.L., Vranjes-Wessely, S., Sachsenhofer, R.F., Schmatz, J., Li, J., Zou, C., 2019. Solid bitumen in shales: petrographic characteristics and implications for reservoir characterization. International Journal of Coal Geology, 205, 14-31.

Mo, H.-J., Huang, W.-L., Machnikowska, H., 2008. Generation and expulsion of petroleum from coal macerals visualized in-situ during DAC pyrolysis. International Journal of Coal Geology, 73, 167-184.

Neumann, V., 2007. Numerical modeling and phase prediction in deep overpressured basinal settings of the Central Graben, North Sea. PhD thesis, Technical University Berlin, Berlin (Germany), 161p.

Peters, K.E., 1986. Guidelines for Evaluating Petroleum Source Rock Using Programmed Pyrolysis. AAPG Bulletin, 70, 318-329.

Petersen, H.I., Holme, A.C., Thomsen, E., Whitaker, M.F., Brekke, T., Bojesen-Koefoed, J.A., Hansen, K.H., Larsen, B.T., 2011. Hydrocarbon potential of Middle Jurassic coaly and lacustrine and Upper Jurassic-lowermost Cretaceous marine source rocks in the Søgne Basin, North Sea. Journal of Petroleum Geology 34, 277-304.

Poetz, S., Horsfield, B., Wilkes, H., 2014. Maturity-driven generation and transformation of acidic compounds in the organic-rich Posidonia shale as revealed by electrospray ionization fourier transform ion cyclotron resonance mass spectrometry. Energy & Fuels, 28, 4877-4888.

Ross, D.J.K., Bustin, M.R., 2009. The importance of shale composition and pore structure upon gas storage potential of shale gas reservoirs. Marine and Petroleum Geology, 26, 916-927.

Rossland, A., Escalona, A., Rolfsen, R., 2013. Permian–Holocene tectonostratigraphic evolution of the Mandal High, Central Graben, North Sea. AAPG Bulletin, 97, 923-957.

Sing, K., 2001. The use of nitrogen adsorption for the characterisation of porous materials. Colloids and Surfaces A: Physicochemical and Engineering Aspects, 187/188, 3-9.

Vandenbroucke, M., Largeau, C., 2007. Kerogen origin, evolution and structure. Organic Geochemistry, 38, 719-833.

Xie, X., Amann-Hildenbrand, A., Littke, R., Krooss, B.M., Li, M., Li, Z., Huang, Z., 2019. The influence of partial hydrocarbon saturation on porosity and permeability in a palaeogene lacustrine shale-hosted oil system of the Bohai Bay Basin, Eastern China. International Journal of Coal Geology, in press. https://doi.org/10.1016/j.coal.2019.03.010

Ziegler, P., 1990. Tectonic and paleogeographic development of the North Sea rift system. In: Blundell, D., Gibbs, A. (Eds.), Tectonic Evolution of the North Sea Rifts. Oxford Science Publications, Oxford (United Kingdom), 1-36.

Ziegs, V., Horsfield, B., Skeie, J.E., Rinna, J., 2017. Petroleum retention in the Mandal Formation, Central Graben, Norway. Marine and Petroleum Geology, 83, 195-214.

Ziegs, V., 2018. Compositional alterations of petroleum as a result of expulsion and migration in the North Sea Central Graben petroleum system. PhD thesis, Technical University Berlin, Berlin (Germany), 172p. https://depositonce.tu-berlin.de//handle/11303/8188